



**Modeling Mercury Cadmium Telluride (HgCdTe)
Photodiodes**

by Bahram Zandi, Dragica Vasileska, and Priyalal Wijewarnasuriya

ARL-TR-5033

November 2009

NOTICES

Disclaimers

The findings in this report are not to be construed as an official Department of the Army position unless so designated by other authorized documents.

Citation of manufacturer's or trade names does not constitute an official endorsement or approval of the use thereof.

Destroy this report when it is no longer needed. Do not return it to the originator.

Army Research Laboratory

Adelphi, MD 20783-1197

ARL-TR-5033

November 2009

Modeling Mercury Cadmium Telluride (HgCdTe) Photodiodes

Bahram Zandi and Priyalal Wijewarnasuriya
Sensors and Electron Devices Directorate, ARL

and

Dragica Vasileska
Arizona State University, Tempe AZ 85287-5706

REPORT DOCUMENTATION PAGE			Form Approved OMB No. 0704-0188		
Public reporting burden for this collection of information is estimated to average 1 hour per response, including the time for reviewing instructions, searching existing data sources, gathering and maintaining the data needed, and completing and reviewing the collection information. Send comments regarding this burden estimate or any other aspect of this collection of information, including suggestions for reducing the burden, to Department of Defense, Washington Headquarters Services, Directorate for Information Operations and Reports (0704-0188), 1215 Jefferson Davis Highway, Suite 1204, Arlington, VA 22202-4302. Respondents should be aware that notwithstanding any other provision of law, no person shall be subject to any penalty for failing to comply with a collection of information if it does not display a currently valid OMB control number. PLEASE DO NOT RETURN YOUR FORM TO THE ABOVE ADDRESS.					
1. REPORT DATE (DD-MM-YYYY) November 2009		2. REPORT TYPE Progress		3. DATES COVERED (From - To)	
4. TITLE AND SUBTITLE Modeling Mercury Cadmium Telluride (HgCdTe) Photodiodes			5a. CONTRACT NUMBER		
			5b. GRANT NUMBER		
			5c. PROGRAM ELEMENT NUMBER		
6. AUTHOR(S) Bahram Zandi, Dragica Vasileska, and Priyalal Wijewarnasuriya			5d. PROJECT NUMBER		
			5e. TASK NUMBER		
			5f. WORK UNIT NUMBER		
7. PERFORMING ORGANIZATION NAME(S) AND ADDRESS(ES) U.S. Army Research Laboratory ATTN: RDRL-SEE-I 2800 Powder Mill Road Adelphi, MD 20783-1197			8. PERFORMING ORGANIZATION REPORT NUMBER ARL-TR-5033		
9. SPONSORING/MONITORING AGENCY NAME(S) AND ADDRESS(ES)			10. SPONSOR/MONITOR'S ACRONYM(S)		
			11. SPONSOR/MONITOR'S REPORT NUMBER(S)		
12. DISTRIBUTION/AVAILABILITY STATEMENT Approved for public release; distribution unlimited.					
13. SUPPLEMENTARY NOTES					
14. ABSTRACT Mercury cadmium telluride (HgCdTe) infrared detectors have been intensively developed over the past 40 years since the first synthesis of this compound semiconductor in 1958. Today, HgCdTe is the most widely used infrared detector material. In this work, we present Silvaco simulations of HgCdTe photodetectors that take into account the temperature dependence of all important material parameters, including bandgap, effective masses, dielectric constant, minority carrier lifetimes, Auger coefficients, etc. As such, this represents the most extensive calculation using Silvaco ATLAS for modeling HgCdTe photodetectors. Optimum detector responsivity and detectivity is obtained by investigating a matrix of photodetectors with different composition, doping, and junction depth.					
15. SUBJECT TERMS Modeling semiconductor materials					
16. SECURITY CLASSIFICATION OF:			17. LIMITATION OF ABSTRACT UU	18. NUMBER OF PAGES 16	19a. NAME OF RESPONSIBLE PERSON Bahram Zandi
a. REPORT Unclassified	b. ABSTRACT Unclassified	c. THIS PAGE Unclassified			19b. TELEPHONE NUMBER (Include area code) (301) 394-2091

Contents

List of Figures	iv
List of Tables	iv
1. Introduction	1
2. HgCdTe Material	1
3. Other Important Parameters for Photodetector Analysis	4
4. Silvaco Simulation Software—General Characteristics	4
5. Silvaco Simulations of HgCdTe Photodetectors	7
6. Future Work	8
7. References	9
Distribution List	10

List of Figures

Figure 1. Bandgap and corresponding spectral cutoff for representative alloy compositions of $\text{Hg}_{1-x}\text{Cd}_x\text{Te}$ as a function of temperature as calculated from equation 1.....	2
Figure 2. Optical absorption coefficient of $\text{Hg}_{1-x}\text{Cd}_x\text{Te}$ as a function of composition x (4).....	3
Figure 3. Comparison of the bandgap vs. lattice constant variation with alloy composition for $\text{Hg}_{1-x}\text{Cd}_x\text{Te}$ and CdZnTe substrates, with the lattice constant for a variety of III-V compounds (5). $\text{Cd}_{0.96}\text{Zn}_{0.04}\text{Te}$ is a good match for a wide range of medium wavelength infrared (MWIR) to LWIR HgCdTe alloys.....	3
Figure 4. ATLAS inputs and outputs.....	5
Figure 5. Dark current of the HgCdTe photodetector evaluated at $T=78\text{ K}$	8

List of Tables

Table 1. ATLAS command groups with the primary statements in each group.....	6
--	---

1. Introduction

Mercury cadmium telluride (HgCdTe) was first synthesized in 1958 by a research group led by Lawson (*1*) at the Royal Radar Establishment in England. This work was the successful outcome of a deliberate effort to engineer a direct-bandgap, intrinsic semiconductor for the long wavelength infrared (LWIR) spectral region (8–14 μm). Early recognition of the significance of this work led to intensive development in a number of countries including the United Kingdom, France, Germany, Poland, the former Soviet Union, and the United States (*2*). Little has been written about the early development years—the existence of work going on in the United States was classified until the late 60s. The French pavilion at the 1967 Montreal Expo illustrated a carbon dioxide (CO_2) laser system with a photovoltaic HgCdTe detector. Photoconductive devices had been built in the United States as early as 1964 at Texas Instruments.

The advancement of crystal growth technology has proceeded deliberately and steadily for four decades in spite of the high vapor pressure of Hg at the melting point of HgCdTe and the known toxicity of the material. HgCdTe has inspired the development of three “generations” of detector devices. The first generation, linear arrays of photoconductive detectors, has been produced in large quantities and is in widespread use today. The second generation, two-dimensional arrays of photovoltaic detectors, is now in high-rate production—thousands of arrays are created annually. Third-generation devices encompass the more exotic device structures embodied in two-color detectors, avalanche photodiodes, and hyperspectral arrays, and are now fielded in demonstration programs. These devices offer functionality beyond today’s detectors, but are some years away from high-rate production. Even as third-generation detector development proceeds, device performance is being enhanced in a number of directions: array size, cooling requirements, long wavelength application of photovoltaic technology, three-color, and readout capability.

2. HgCdTe Material

Several properties of HgCdTe qualify it as highly useful for infrared detection:

- Adjustable bandgap from 0.7 to 25 μm .
- Direct bandgap with a high absorption coefficient.
- Moderate dielectric constant/index of refraction.
- Moderate thermal coefficient of expansion.
- Availability of wide bandgap lattice-matched substrates for epitaxial growth.

We now discuss each of these key properties.

Infrared detection in HgCdTe begins with the excitation of an electron from the valence band into the conduction band. The minimum photon energy required is equal to the bandgap, E_g . The bandgap of Hg $_{1-x}$ Cd $_x$ Te is a function of the alloy composition ratio “ x ” of CdTe to HgTe and the temperature of the material. A number of equations have been developed to summarize the empirically measured relationship. One of these, developed by Hansen et al. (3), is given by the expression

$$E_g(T) = -0.302 + 1.93x - 0.81x^2 + 0.832x^3 + 5.35 \times 10^{-4}(1 - 2x)T \quad (\text{eV}). \quad (1)$$

Figure 1 illustrates the dependence of this equation for representative compositions of the alloy, $x = 0.2, 0.3,$ and 0.4 , which span the medium-to-long wavelength spectral regions, 3–14 μm . With higher values of x , the spectral response can be tailored to wavelengths as short as 0.7 μm , corresponding to the bandgap of CdTe. Since the bandgap of HgTe is negative, or inverted, the alloy can be grown to achieve arbitrarily small bandgaps. In practice, HgCdTe has not been used significantly beyond about 25 μm .

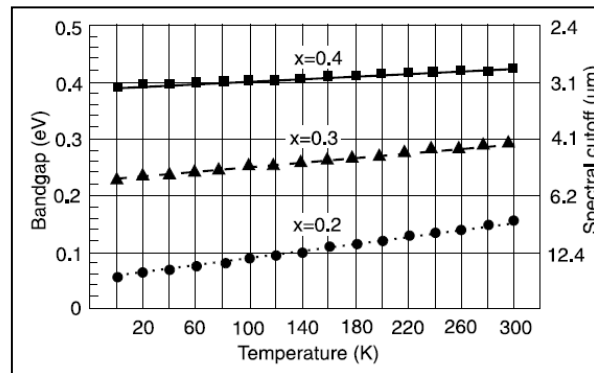


Figure 1. Bandgap and corresponding spectral cutoff for representative alloy compositions of Hg $_{1-x}$ Cd $_x$ Te as a function of temperature as calculated from equation 1.

Direct bandgap semiconductors, such as HgCdTe, have a sharp onset of optical absorption as the photon energy increases above E_g . In contrast, indirect semiconductors, such as silicon or germanium, have softer absorption curves. The optical absorption coefficient for HgCdTe has been measured by Scott (4) and is illustrated in figure 2 for a wide range of alloy compositions. Strong optical absorption allows HgCdTe detector structures to absorb a very high percentage of the signal while being relatively thin, on the order of 10–20 μm . Minimizing the detector thickness helps to minimize the volume of material which can generate noise, thermal excess carriers, in the diffusion-limited operating mode.

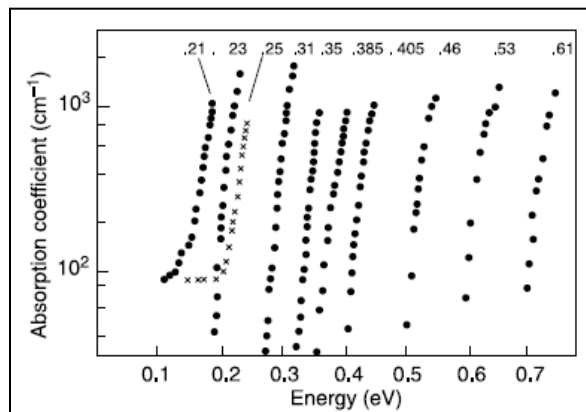


Figure 2. Optical absorption coefficient of $\text{Hg}_{1-x}\text{Cd}_x\text{Te}$ as a function of composition x (4).

The final key property we address is the availability of lattice-matched substrates for epitaxial growth. Epitaxial growth is now used almost exclusively for HgCdTe detector array production. About 15 years ago, it was found that the crystal perfection and surface morphology of the epitaxial layers was significantly influenced by the substrate-epitaxial layer lattice constant mismatch. This was discovered when about 4% ZnTe was added to CdTe to tune the substrate lattice constant to match HgCdTe . A great advantage of this II-VI alloy system is the narrow range of lattice constant variation from CdTe to HgTe , as illustrated in figure 3.

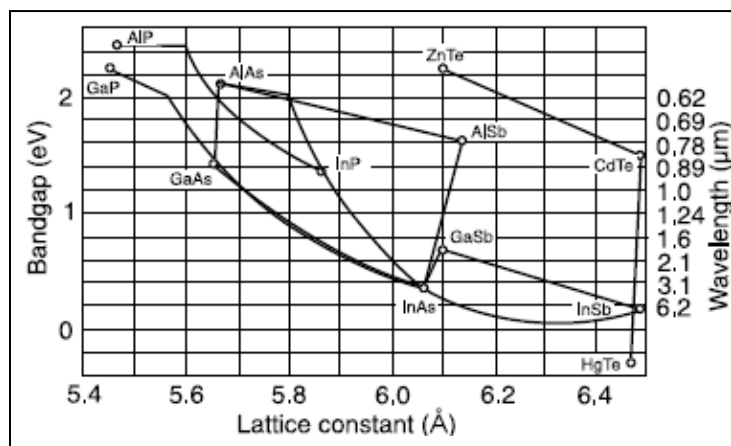


Figure 3. Comparison of the bandgap vs. lattice constant variation with alloy composition for $\text{Hg}_{1-x}\text{Cd}_x\text{Te}$ and CdZnTe substrates, with the lattice constant for a variety of III-V compounds (5). $\text{Cd}_{0.96}\text{Zn}_{0.04}\text{Te}$ is a good match for a wide range of medium wavelength infrared (MWIR) to LWIR HgCdTe alloys.

3. Other Important Parameters for Photodetector Analysis

With regard to other important parameters for photodetector analysis, we first give here the effective electron and hole masses (6):

$$m_e / m_0 = \left[-0.6 + 6.333 \left(\frac{2}{E_g(T)} + \frac{1}{E_g(T)+1} \right) \right]^{-1} \quad (2)$$
$$m_h / m_0 = 0.55$$

The effective electron and hole masses directly affect the effective electron and hole density of states in the Silvaco simulation framework.

Other critical parameter is the dielectric constant, which enters in the solution of the Poisson equation. The relative dielectric constant dependence upon composition is given as (6)

$$\kappa_s = 20.5 - 15.5x + 5.7x^2 \quad (3)$$

Wijewarnasuriya (7) provided the minority carrier lifetimes and the Auger generation/recombination coefficients.

4. Silvaco Simulation Software—General Characteristics

ATLAS is a modular and extensible framework for one-, two-, and three-dimensional semiconductor device simulation (8). It is implemented using modern engineering practices that promote robustness, reliability, and maintainability. ATLAS should only be used with Virtual Wafer Fab (VWF) Interactive Tools, which include DeckBuild, TonyPlot, DevEdit, MaskViews, and Optimizer. DeckBuild provides an interactive runtime environment. TonyPlot supplies scientific visualization capabilities. DevEdit is an interactive tool for structure and mesh specification and refinement. MaskViews is an integrated circuit (IC) layout editor. The Optimizer supports blackbox optimization across multiple simulators. ATLAS is very often used in conjunction with the ATHENA process simulator. ATHENA predicts the physical structures that result from processing steps. The resulting physical structures are used as input by ATLAS, which then predicts the electrical characteristics associated with specified bias conditions. The combination of ATHENA and ATLAS makes it possible to determine the impact of process parameters on device characteristics.

Figure 4 shows the types of information that flow in and out of ATLAS. Most ATLAS simulations use two inputs: a text file that contains commands for ATLAS to execute and a structure file that defines the structure that will be simulated. ATLAS produces three types of

output. The runtime output provides a guide to the progress of simulations running and is where error messages and warning messages appear. Log-files store all terminal voltages and currents from the device analysis, and solution files store two- and three-dimensional data relating to the values of solution variables within the device for a single bias point.

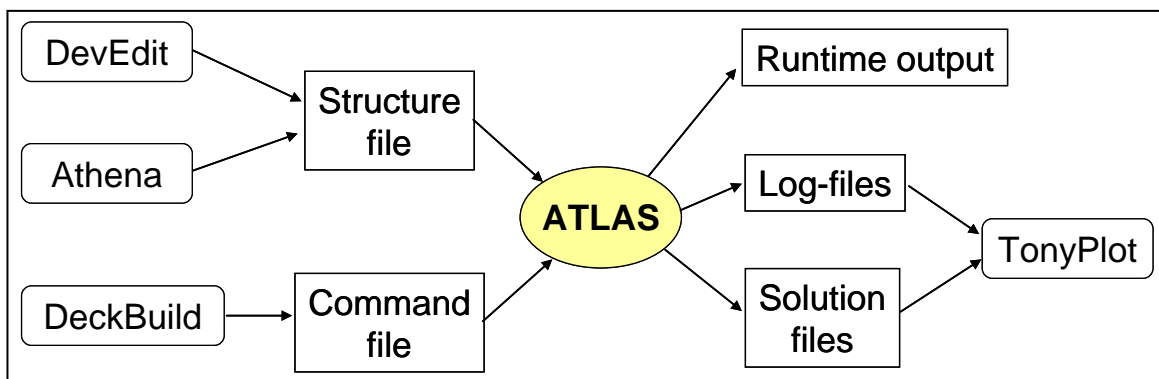


Figure 4. ATLAS inputs and outputs.

An ATLAS command file is a list of commands for ATLAS to execute. This list is stored as an ASCII text file that can be prepared in DeckBuild or using any text editor. Preparation of the input file in DeckBuild is preferred, and can be made easier by appropriate use of the DeckBuild Commands menu. The input file contains a sequence of statements. Each statement consists of a keyword that identifies the statement and a set of parameters. The general format is

<STATEMENT> <PARAMETER>=<VALUE>

Some hints on the proper structure of the statements are listed below:

1. The statement keyword must come first, but after this the order of parameters within a statement is not important.
2. It is only necessary to use enough letters of any parameter to distinguish it from any other parameter on the same statement. Thus, CONCENTRATION can be shortened to CONC. However, REGION cannot be shortened to R since there is also a parameter RATIO associated with the DOPING statement.
3. Logicals can be explicitly set to false by preceding them with the ^ symbol.
4. Any line beginning with # is ignored. These lines are used as comments.
5. ATLAS can read up to 256 characters on one line; however, it is best to spread long input statements over several lines to make the input file more readable. The character \ at the end of a line indicates continuation.

The order in which statements occur in an ATLAS input file is important. There are five groups of statements, and these must occur in the correct order. These groups are indicated in table 1. **Each input file must contain these five groups in order.** Failure to do this will usually cause an error message and termination of the program, but it could lead to incorrect operation of the program. For example, material parameters or models set in the wrong order may not be used in the calculations. The order of statements within the mesh definition, structural definition, and solution groups is also important.

Table 1. ATLAS command groups with the primary statements in each group.

Group		Statements
1. Structure Specification	_____	MESH REGION ELECTRODE DOPING
2. Material Models Specification	_____	MATERIAL MODELS CONTACT INTERFACE
3. Numerical Method Selection	_____	METHOD
4. Solution Specification	_____	LOG SOLVE LOAD SAVE
5. Results Analysis	_____	EXTRACT TONYPLOT

A device structure can be defined in three different ways in ATLAS:

- An existing structure can be read in from a file. The structure can be created by an earlier ATLAS run or by another program such as ATHENA or DevEdit. A single statement loads in the mesh, geometry, electrode positions, and DOPING of the structure. This statement is `MESH INFILE=<filename>`.
- The input structure can be transferred from ATHENA or DevEdit through the automatic interface feature of DeckBuild.
- A structure can be constructed using the ATLAS command language.

The first and second methods are more convenient than the third and are to be preferred whenever possible.

Several different numerical methods can be used for calculating the solutions to semiconductor device problems. Different solution methods are optimum in different situations and some guidelines will be given here. Different combinations of models will require ATLAS to solve up to six equations. For each of the model types there are basically three types of solution techniques: (1) de-coupled (Gummel), (2) fully coupled (Newton), and (3) Block. In simple terms, the de-coupled technique like the Gummel method will solve for each unknown in turn, keeping the other variables constant and repeating the process until a stable solution is achieved. Fully coupled techniques such as the Newton method solve the total system of unknowns together. The combined or Block methods will solve some equations fully coupled, while others are de-coupled.

In general, the Gummel method is useful where the system of equations is weakly coupled, but has only linear convergence. The Newton method is useful when the system of equations is strongly coupled and has quadratic convergence. The Newton method may, however, spend extra time solving for quantities that are essentially constant or weakly coupled. Newton also requires a more accurate initial guess to the problem to obtain convergence. Thus, a Block method can provide for faster simulation times in these cases over Newton. Gummel can often provide better initial guesses to problems. It can be useful to start a solution with a few Gummel iterations to generate a better guess and then switch to Newton to complete the solution. Specification of the solution method is carried out as follows:

METHOD GUMMEL BLOCK NEWTON

5. Silvaco Simulations of HgCdTe Photodetectors

When numerically modeling optical photodetectors, the first thing that needs to be specified is the device structure. Then, after the structure, the theoretical model parameters, and the solution methods are specified, the dark current of the HgCdTe photodetector is calculated. A plot of the dark current versus applied bias is given in figure 5. The dark current characteristic shown in figure 5 is for a temperature of 78 K and the obtained values agree with theoretical predictions.

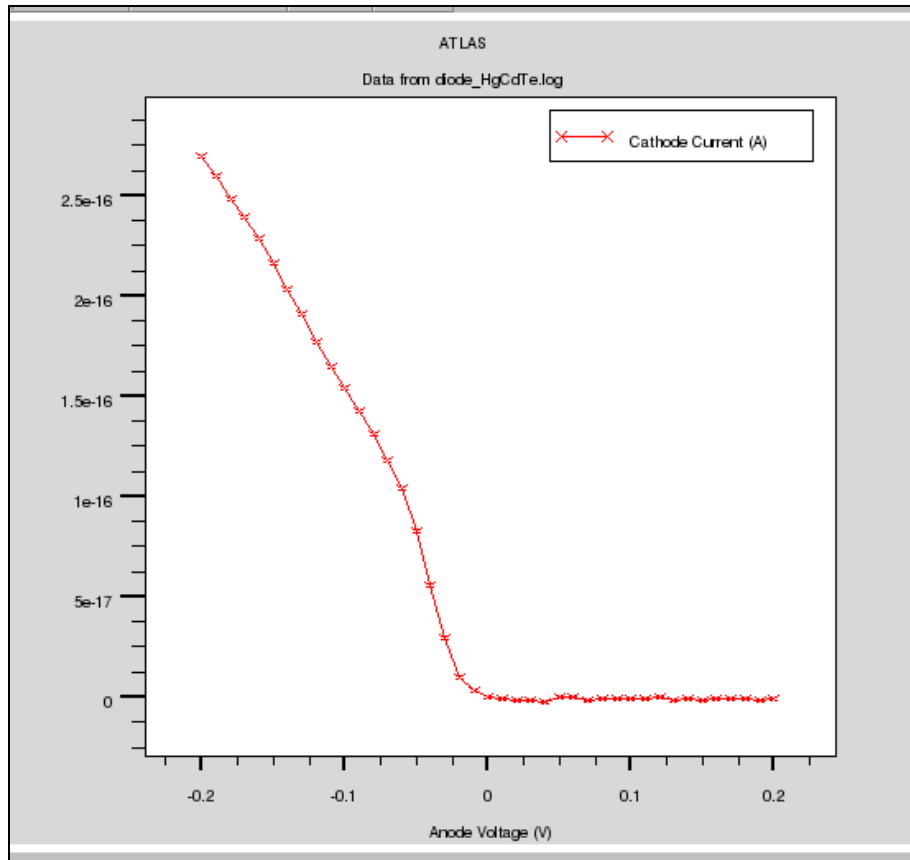


Figure 5. Dark current of the HgCdTe photodetector evaluated at T=78 K.

6. Future Work

The work presented in section 5 will be continued to extract the external and the internal quantum efficiency, responsivity, and the detectivity of the photodetectors. An array of photodetectors with different geometries will then be used to find a photodetector with optimum performance parameters given the application of interest.

7. References

1. Lawson, W. D.; Nielson, S.; Putley, E. H.; Young, A. S. Preparation and Properties of HgTe and Mixed Crystals of HgTe-CdTe. *J. Phys. Chem. Solids* **1959**, *9*, 325–329.
2. Long, D.; Schmidt, J. L. Mercury-cadmium Telluride and Closely Related Alloys. *Semiconductors and Semimetals* **1970**, *5*, 175–255, Willardson, R. K.; Beer, A. C., eds., Academic Press, New York.
3. Hansen, G. L.; Schmidt, J. L.; Casselman, T. N. Energy Gap Versus Alloy Composition and Temperature in Hg_{1-x}CdxTe. *J. Appl. Phys.* **1982**, *53*, 7099–7101.
4. Scott, M. W. Energy Gap in Hg_{1-x}CdxTe by Optical Absorption. *J. Appl. Phys.* **1969**, *40*, 4077–4081.
5. Shur, A. *Microdevices, Physics and Fabrication Technologies*; Plenum Press: New York, 1995.
6. Silvaco Web page. www.silvaco.com (accessed 2009).
7. Wijewarnasuriya, P. Private communications, 2009.
8. *ATLAS User's Manual*, Ed. 6, Silvaco International: Santa Clara, CA, 1998.

<u>No. of</u> <u>Copies</u>	<u>Organization</u>	<u>No. of</u> <u>Copies</u>	<u>Organization</u>
1 ELEC	ADMNSTR DEFNS TECHL INFO CTR ATTN DTIC OCP 8725 JOHN J KINGMAN RD STE 0944 FT BELVOIR VA 22060-6218	1	COMMANDER US ARMY RDECOM ATTN AMSRD AMR W C MCCORKLE 5400 FOWLER RD REDSTONE ARSENAL AL 35898-5000
1	DARPA ATTN IXO S WELBY 3701 N FAIRFAX DR ARLINGTON VA 22203-1714	1	US GOVERNMENT PRINT OFF DEPOSITORY RECEIVING SECTION ATTN MAIL STOP IDAD J TATE 732 NORTH CAPITOL ST NW WASHINGTON DC 20402
1 CD	OFC OF THE SECY OF DEFNS ATTN ODDRE (R&AT) THE PENTAGON WASHINGTON DC 20301-3080	1	ARIZONA STATE UNIV DEPT OF ELECTRICAL ENGINEERING ATTN D VASILESKA IRA A FULTON SCHOOL OF ENGINEERING TEMPE AZ 85287-5706
1	US ARMY RSRCH DEV AND ENGRG CMND ARMAMENT RSRCH DEV AND ENGRG CTR ARMAMENT ENGRG AND TECHNLGY CTR ATTN AMSRD AAR AEF T J MATTS BLDG 305 ABERDEEN PROVING GROUND MD 21005-5001	1	US ARMY RSRCH LAB ATTN RDRL CIM G T LANDFRIED BLDG 4600 ABERDEEN PROVING GROUND MD 21005-5066
1	PM TIMS, PROFILER (MMS-P) AN/TMQ-52 ATTN B GRIFFIES BUILDING 563 FT MONMOUTH NJ 07703	6	US ARMY RSRCH LAB ATTN AMSRD ARL SE EI P WIJEWARNASURIYA ATTN IMNE ALC HRR MAIL & RECORDS MGMT ATTN RDRL CIM L TECHL LIB ATTN RDRL CIM P TECHL PUB ATTN RDRL SEE I B ZANDI ATTN RDRL SEE I P UPPAL ADELPHI MD 20783-1197
1	US ARMY INFO SYS ENGRG CMND ATTN AMSEL IE TD A RIVERA FT HUACHUCA AZ 85613-5300		

TOTAL: 16 (1 ELEC, 1 CD, 14 HCS)